ELSEVIER

Physics of the Earth and Planetary Interiors 117 (2000) 153–170

PHYSICS OF THE EARTH AND PLANETARY INTERIORS

www.elsevier.com/locate/pepi

Laboratory experiments on high Rayleigh number thermal convection in a rapidly rotating hemispherical shell

Ikuro Sumita *, Peter Olson

Department of Earth and Planetary Sciences, The Johns Hopkins University, Baltimore, MD 21218, USA

Received 30 October 1998; accepted 26 May 1999

Abstract

We report the results of laboratory experiments on high Rayleigh number thermal convection in a rotating hemispherical shell at Ekman number of $Ek = 4.7 \times 10^{-6}$. We use the combined effect of centrifugal acceleration and laboratory gravity in the lower hemisphere of a spherical shell to simulate the gravity in the Earth's core. Visualization and recording of the pattern and flow, together with the measurements of temperature time series, are used to quantify the motions. We study the change in the convective pattern and temperature structure vs. the Rayleigh number, Ra, up to 45 times the critical value Ra_c. Three major regimes are found. For $Ra/Ra_c < 1$ (regime i), the hemisphere is stably stratified. Zonal motion exists in this regime in the form of interleaved lenses of retrograde and prograde flows. For $1 < Ra/Ra_c < 8$ (regime ii), we observe penetrative convection, driven by prograde spiralling cold plumes that originate from the inner core and form a closely spaced columnar structure. These plumes slowly drift retrograde, advected by the mean zonal flow. For $Ra/Ra_c > 8$ (regime iii), we observe dual convection, driven by cold plumes from the inner boundary and by warm plumes from the outer boundary. This produces a very fine-scaled geostrophic turbulence. A retrograde flow, fastest near the inner boundary, is present in this regime, perhaps driven by Reynolds stresses. The transition from (ii) to (iii) is caused by difference in the wave number of the plumes originating from the inner and outer boundaries, i.e., the cold plumes from the inner boundary have smaller wave numbers as compared to warm plumes from the outer boundary, owing to differences in the outer boundary slope. Temperature measurements by thermistor probes indicate oscillations with a typical period corresponding to the azimuthal drift of columnar structures past the fixed probes, as well as nonsinusoidal features arising from nonlinearity. Convection is the main form of heat transfer in most of the range covered, and is pronounced in the equatorial region. Under the assumption of geostrophic balance, we suggest several new interpretations for convection in the Earth's core.

Keywords: Rotating; Spherical shell; Thermal convection; High Rayleigh number; Earth's core

1. Introduction

Convection in the Earth's core is strongly influenced by rotation and is characterized by a very small Ekman number (Ek). In order to initiate convection in this regime, the Rayleigh number (Ra) must be quite high. In spite of recent success, this regime is still remote from numerical computations of convection and dynamo action in a rotating sphere. On the other hand, laboratory experiments of rotating convection are capable of achieving regimes where

* Corresponding author. Tel.: +1-410-516-7034; fax: +1-410-516-7933; e-mail: sumita@ekman.eps.jhu.edu

0031-9201/00/$ - see front matter
PII: S0031-9201(99)00094-1

these two parameters are more extreme, by roughly an order of magnitude, compared to numerical calculations. We report here the characteristics of finite amplitude thermal convection in a rotating hemispherical shell at a low Ekman number and show how the structure of the convection changes as the Rayleigh number is increased.

Rotating convection experiments use the combined effects of laboratory gravity and centrifugal gravity in the lower hemisphere of a spherical shell to simulate radially directed gravity. The technique was first used by Cordero and Busse (1992) and Cordero (1993), and later by Busse et al. (1997). In these studies, visualization of the flow pattern and recording of the temperature time series were made for Ekman number of $Ek \simeq 10^{-5}$–10^{-2} and Rayleigh number of $Ra \simeq 10^{3}$–10^{6}, which is up to four times critical. They observe nearly periodic, columnar convection in this parameter regime. These studies also observe quasi-periodic temperature fluctuations, which increase in frequency with the Rayleigh number. They attribute the fluctuations to the combined effect of propagation of thermal Rossby wave and advection of the columnar vortices by a retrograde thermal wind whose strength depends on the Rayleigh number.

In order to extend the experimental investigation of rotating spherical convection to more extreme parameters, we have built an apparatus similar to Cordero and Busse but larger in size and capable of rotating at a higher rate. With this device, we reach both lower Ekman numbers (4.7×10^{-6}) and higher Rayleigh numbers (8.1×10^{8}), which is approximately 45 times the critical value at this Ekman number. Using this apparatus, we examine a large range of Rayleigh numbers, allowing a closer approach to conditions in the Earth's core. Our apparatus has an inner and outer core radius ratio of 1:3, similar to the Earth's core, as compared to the thinner shell ratios of 1:1.3 or 1:1.8 used in previous studies. As compared to a sphere, a hemisphere is easier for observing the planform, and also permits placing temperature probes in the interior of the shell. We record the instantaneous convective pattern as well as its time evolution. We also record temperature fluctuations in the fluid, and estimate flow velocities using tracer dyes. Using these visualization and measurement schemes together, we define several styles of convection at high Rayleigh number which are quite different from convection nearer to the critical Rayleigh number, and we characterize their spatial and temporal scales.

In this paper, we first show the results of the pattern visualization and flow measurements and classify the major regimes. We then present the analyzed results of the corresponding temperature measurements. Finally, an interpretation is made of the flow mechanics, and its implications for convection in the Earth's core are discussed.

2. Experimental technique

The experimental apparatus is modified from that used by Cardin and Olson (1992; 1994) and Manneville and Olson (1996). It consists of an outer hemisphere 30 cm in diameter with a thickness of 0.84 mm, and a concentric inner sphere 10 cm in diameter, both made of copper. The outer hemisphere is in the ''southern hemisphere'' position as shown in Fig. 1. A plexiglass lid of thickness 0.95 cm is attached to the outer hemisphere in the position of the equatorial plane to allow viewing of the fluid motion from above. Because of the large difference in the thermal conductivity of the plexiglass and copper, the conductive heat flux across the plexiglass lid is approximately four orders of magnitude smaller than that across the copper sphere, and is therefore negligible. Both the outer hemisphere and the inner sphere are fixed to a stainless steel shaft, which serves as a rotation axis for the shell and also provides a conduit along which cooling fluid is circulated through the inner sphere. The portion of the shaft within the lower hemisphere and in contact with the working fluid is insulated with rubber in order to minimize the heat transfer directly from the shaft to the fluid. The outer sphere is kept at the constant room temperature ~ 20°C. By adjusting the temperature of the cooling fluid, a temperature difference up to ~ 12°C can be maintained across the hemispherical shell. The shaft rotation rate, constant to the order of one part in 10^{4}, is regulated by a servo motor. Coupling is provided and is linked by a pulley and belt assembly. We use water as the working fluid.

Two visualization methods are used. Kalliroscope flakes are mixed into the working fluid, which orient

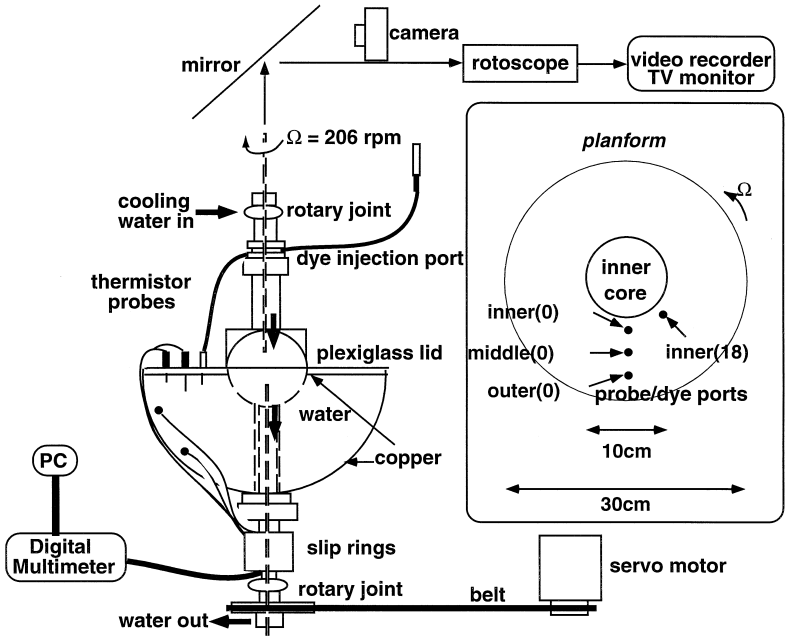

Fig. 1. Sketch of the experimental apparatus.

in the flow and reveal the pattern of shear. In addition to flakes, we also inject fluorescent dye into the working fluid at selected points, which acts as a tracer. The time evolution of the convection planform is imaged using a video recording system. A mirror is placed at an angle of 45° above the hemisphere and a video recording of the flow pattern near the equatorial plane is made through an optically aligned rotoscope device, which removes the rotation from the video image. The instantaneous convective pattern is imaged with flash photography, using illumination from two strobes placed around the hemisphere, 180° apart. In addition to planform, we use stroboscopic light to observe convective motion from oblique angles.

Hypodermic thermistor probes are used for temperature measurements in the fluid. An array of probes are placed 3.1, 5.6, 8.1 cm from the inner boundary (ICB), and two surface probes are placed at latitudes of 10° and 50° at the outer boundary (CMB). The depth of the individual probes in the array can be adjusted to record temperatures at various depths beneath the equatorial plane. Thermistor signals, recorded at 1-s intervals, are passed through a set of slip rings mounted on the rotating shaft and are recorded by a PC in the lab frame. The cooling fluid is transmitted to the rotating shaft through a pair of rotary joints. Its temperature is measured at the entrance and exit of the inner core. The temperature difference at these two points provides a measurement of the total heat flux at the ICB. We use the temperature of the cooling fluid at exit of the inner core to define the temperature at the ICB. We define temperature at the CMB using the thermistor located at 10° on the CMB.

The experimental procedure is as follows. The hemisphere is spun up to a fixed rotation rate of 206 rpm, and the temperature difference is imposed by circulating the coolant through the inner core. Since the centrifugal force acts outwards from the rotation axis, fixing the inner core temperature below the temperature of the working fluid creates positive buoyancy at the ICB and initiates convection. We use the term *adverse* for the temperature gradient established this way. In contrast, fixing the inner core at a temperature above the working fluid results in negative buoyancy at the ICB and inhibits convection. We use the term *reverse* for the temperature gradient in this situation. Temperature and flow pattern are monitored to determine when spin-up is

complete and whether the time-averaged state reaches stationarity, which is typically 30 to 120 min. The turnover time of meridional and zonal circulations were measured to be ~ 10 and 90 min, respectively, for $Ra/Ra_c \sim 8$, and 1.3 and 24 min, respectively, for $Ra/Ra_c \sim 42$. The zonal circulation time can be regarded to be the time required to establish the steady state, which is comparable to that determined from the visual observation and temperature measurements. The importance of advection for achieving stationarity is verified by the large Péclet number calculated using zonal flow: 85 for $Ra/Ra_c = 8$, and 312 for $Ra/Ra_c = 42$. After this condition is reached, we begin visual recording, the injection and tracking of dye, and temperature recording. Since injection of dye can locally alter temperature and buoyancy, the experiments for temperature measurements and dye injection are done separately.

The relevant experimental parameters are summarized in Table 1. The definition of gravity in the experiment requires some care. The equipotential surfaces of the effective gravity are parabolic and for a rotation rate of 206 rpm, at the outer sphere, the effective radial gravity at the equator is seven times that at the pole, resulting in a cylindrical distribution of effective gravity. The effective gravity at the outer sphere has a tangential component directed toward the pole for latitudes less than 8°, and a tangential component directed toward the equator for latitudes larger than 8°. Since the cylindrical component of the gravity is known to be the primary driving force of convection at low Ekman numbers (Busse, 1970; Glatzmaier and Olson, 1993), we propose that flows generated with this gravity distribution closely approximate the flows generated with purely radial gravity in spite of these deviations.

3. Results

3.1. Convective pattern and flow

From the visualizations, we identify three basic styles of flow under the fixed Ekman number of 4.7×10^{-6}, which depend on Rayleigh number. These are: (i) flow with stable stratification, (ii) penetrative convection, and (iii) dual convection.

3.1.1. Stably stratified flow

We made a sequence experiments with different inner core temperatures at fixed Ekman number in order to determine the critical adverse temperature difference for onset of convection. We find the critical Rayleigh number (Ra_c) corresponds to a temperature difference of 0.26°C. With the parameters in Table 1, this corresponds to a critical Rayleigh number of $Ra_c = 1.8 \times 10^7$. This value is larger by a factor of three than the critical Rayleigh number $Ra_c = 6.89 \times 10^6$ calculated by Cardin and Olson (1994) for $Ek = 5 \times 10^{-6}$, from a linear stability analysis of a columnar convection in a spherical shell.

When the temperature gradient is adverse but less than critical, and in all cases with reverse temperature gradients, we do not observe radial motion in the form of plumes, vortices or other convective structures. However, there generally is some azimuthal motion, as can be seen in Fig. 2, which consists of interleaved lenses of mainly retrograde moving fluid alternating with lenses of prograde flow.

3.1.2. Penetrative convective regime

For $1 < Ra/Ra_c < 8$, convective motion is initiated at the ICB with an azimuthal wave number of

Table 1
Experimental parameters
$g(\Omega) = D\Omega^2$; α, thermal expansivity; κ, thermal diffusivity; υ, kinematic viscosity; D, shell thickness

Parameter	Experiments	Earth's core
Inner/outer radius ratio	0.33	0.34
Prandtl number: υ/κ	7	0.1–10
Rayleigh number: $(\alpha g(\Omega)\Delta T D^3)/\kappa\upsilon$	-3×10^8–8×10^8	?
Ra/Ra_c[a]	−14–45	?
Ekman number: $\upsilon/\Omega D^2$	4.7×10^{-6}	10^{-15}

[a] $Ra_c = 1.8 \times 10^7$, determined from the experiment.

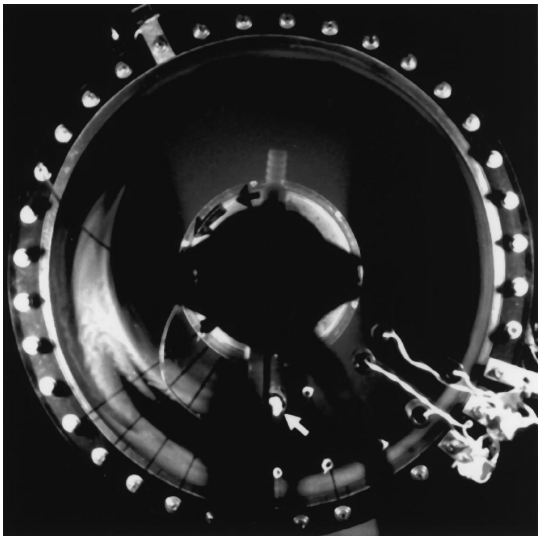

Fig. 2. Planform of the flow pattern in the stably stratified regime at $Ra/Ra_c = -12.6$ ($Ek = 4.7 \times 10^{-6}$). The rotation is counterclockwise. Dye was injected into the working fluid at the point shown by the white arrow. The interleaving lenses of dye indicate the pattern of the azimuthal flow.

typically 16 to 20, as shown in Fig. 3. This wave number is smaller than that predicted by the linear stability analysis of Cardin and Olson (1994), who obtain $m = 26$ at $Ek = 5 \times 10^{-6}$. The image in Fig. 3 is produced by injecting dye in the outer portion of the annular region of the shell, leaving the inner portion undyed. With the growth of the instability, the undyed region penetrates radially outwards in the form of cold plumes, while the dye penetrates inward between the plumes, tracing the return flow. The pattern visualized by flakes is identical to this, which implies that the pattern seen in flakes corresponds to plumes. The instability takes the form of periodic columnar plumes arrayed around the shell. In cross-section, in the equatorial plane, for example, the plumes are tilted in the prograde direction so the whole array forms a prograde spiral. Tilt is a consequence of the sloping spherical CMB effect which generates anticyclonic (cyclonic) vorticities moving away from (towards) axis. Presence of prograde tilt as seen in Fig. 3 argues that the plumes are columnar. From the comparison of the two photographs in Fig. 3 (taken 155 s apart), we find that the pattern drifts slowly retrograde at $\sim 4°$/min. A video recording taken between the times these two photographs were taken, confirms the retrograde drift of the pattern.

At larger Rayleigh numbers, the instability develops more quickly, and the radial extent and the wave number of the plumes increases. At $Ra/Ra_c = 3$, the azimuthal wave number is about ~ 24 and the plumes

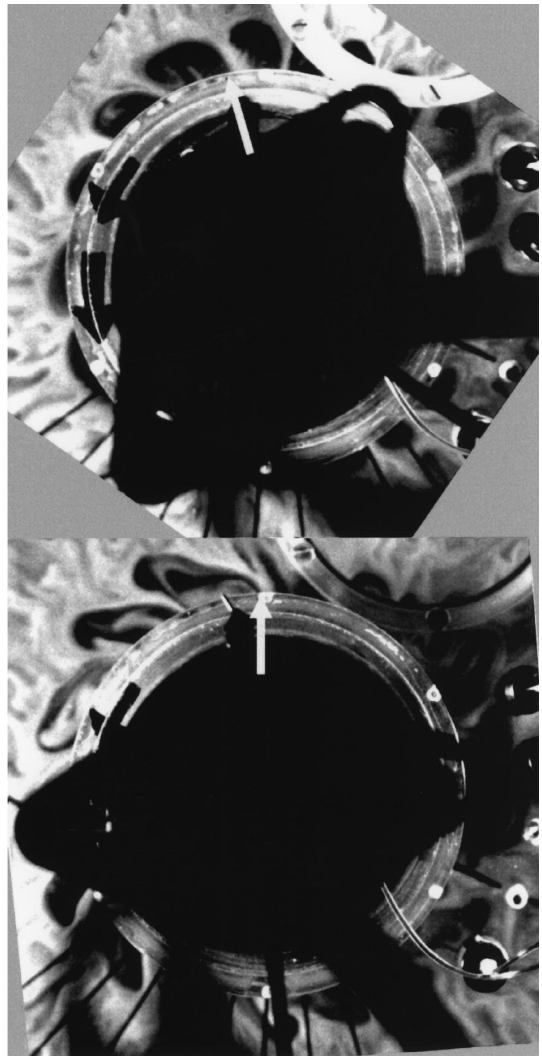

Fig. 3. A close-up image of the flow pattern adjacent to the inner core near the onset of convection at $Ra/Ra_c = 7$ ($Ek = 4.7 \times 10^{-6}$). The prograde tilting cold plumes originating from the inner core appear as dark regions. Narrow return flows are visualized by fluorescent dye and appear as light regions. The bottom photograph was taken 155 s later. The white arrow indicates the retrograde drift of the plumes of approximately 4°/min.

extend from the ICB to the middle of the shell, forming nearly periodic spirals. As can be seen in Fig. 4, at $Ra = 1.1 \times 10^8$ ($Ra/Ra_c = 5.9$) the plumes extend from ICB to the CMB and the azimuthal wave number near the CMB is about 60. At $Ra = 1.3 \times 10^8$ ($Ra/Ra_c = 7.3$), which is the highest Rayleigh number for this regime, the wave number near the CMB is about 72. This is close to the wave number of 73 calculated by Zhang (1992) at $Ra = 1.45 \times 10^8$ and $Ek = 4.5 \times 10^{-6}$. Zhang's model was internal-heated, which results in convection initiated at mid-shell, similar to the situation in Fig. 4, which may explain the agreement. The prograde tilt of the plumes becomes most pronounced near the CMB, where the boundary slope is the steepest. The tilt amounts to approximately 20° in azimuth and agrees well with the results calculated by Zhang (1992). The cold plumes are closely spaced and alternate with narrow warm plumes. Inspection of Fig. 4 shows that the azimuthal wave number increases with distance from the ICB, varying from 24 near the ICB, to 30 at mid-shell and reaching 60 near the CMB. The azimuthal width of the plumes are fairly uniform throughout the shell, but some of the plumes split as they move outwards, increasing the wave number of the pattern with increasing radius.

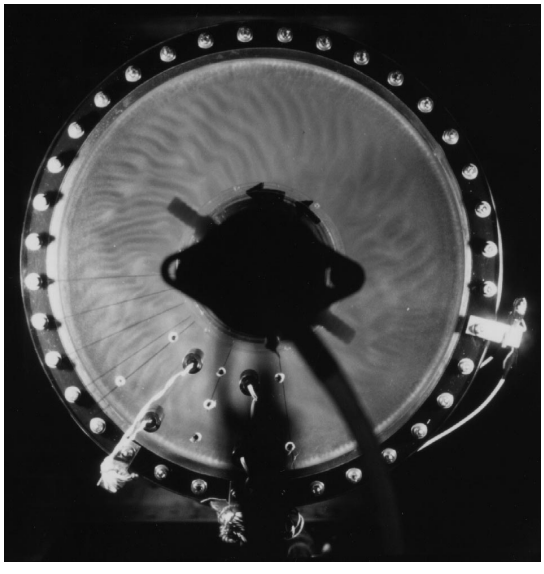

Fig. 4. Spiralling columnar convective pattern visualized by flakes, in the penetrative convection regime at $Ra/Ra_c = 5.9$ ($Ek = 4.7 \times 10^{-6}$).

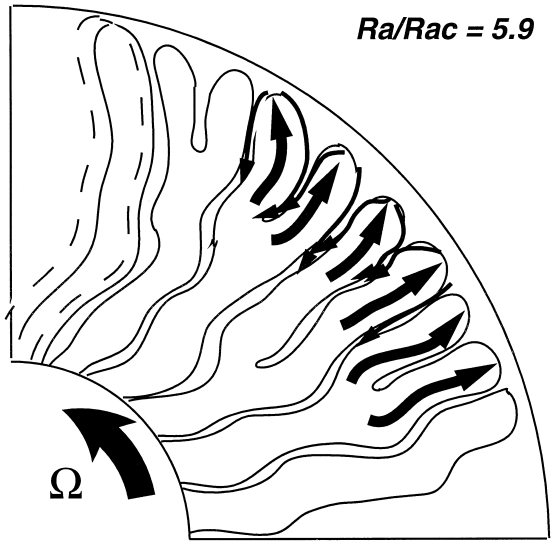

Fig. 5. An interpretive diagram of Fig. 4 showing the flow pattern. The broad arrows correspond to cold plumes. Narrow arrows are the warm return flow.

The interpretive diagram of the flow described here is shown in Fig. 5. In meridional sections, the flow structure is essentially two-dimensional and columnar, as revealed by the pattern of dye streaks observed at oblique angles. A well-defined cylindrical curtain of dye forms at the tangent cylinder and the dye is strongly inhibited from crossing this cylindrical surface. Since the convection is driven by cold plumes originating at the ICB and since the spiral pattern penetrates into the stably stratified outer region of the shell, we call this the *penetrative convective* regime. The interior zonal flow is retrograde throughout the shell, with a typical angular speed of about 3 to 5°/min at $Ra/Ra_c \sim 6$. The maximum zonal flow speed is observed near the middle of the shell, indicating an approximately parabolic velocity profile across the shell.

The flow pattern in individual plumes was visualized by two methods. First, by injecting dye into the fluid and allowing it to become entrained into the convection, dye curtains form around the rim of the cold plumes, as we have seen in Fig. 3. These dye curtains are ultimately incorporated into the plumes along their prograde sides, an effect confirmed by using flakes and dye at the same time. We infer from this behavior that the motion of a typical fluid parcel

in the plume consists of a pair of cyclonic and anticyclonic circulations at its prograde and retrograde sides, respectively, superimposed on a mean retrograde flow. When the dye was injected near the outer sphere, we observe that the dye curtains form on both prograde and retrograde sides of each plume, confirming that each outward moving plume structure in Figs. 3 and 4 includes a pair of vortices with opposing circulation. By observing the tracing of the plumes by the dye rims, we find that the radial flow is faster than the mean zonal flow by a factor of ~ 3 for $Ra/Ra_c \sim 8$.

A second visualization technique consists of injecting dye near the CMB at high latitudes at $Ra/Ra_c \sim 6$. Flow along the convection columns then transports the dyed fluid from the CMB into the interior of the shell. This results in an image in which the interior of the cells are dyed and the rims remain undyed. The dyed vortex cores retain their shape for long intervals of time and slowly drift in the retrograde direction.

Both of the above visualization techniques have confirmed the retrograde drift of the columns. This means that to a good approximation, the fluid particles and the pattern move at the same rate at $Ra/Ra_c \sim 6$, and implies that the retrograde drift of the pattern consists of a zonal flow rather than a phase propagation.

3.1.3. Dual convective regime

For $Ra/Ra_c > 8$, the nearly periodic spiralling columns are replaced by a form of two-dimensional turbulent columnar convection, characterized by a very fine-scale structure in the equatorial plane (see Fig. 6). The transition from the nearly periodic, penetrative convective regime to this regime appears to occur when the cold plumes originating at the ICB extend to the CMB, triggering an instability at the CMB. The instability formed at the CMB has a wave number of around 108. This corresponds to the preferred instability at latitude of 36° according to the linear theory of Busse (1970). This instability consists of columnar cells with a retrograde tilt, for the same reasons as the cells formed at the ICB have a prograde tilt. Because the wave number of plumes originating at the ICB are typically about 72 near CMB, there is a wave number mismatch with the cells originating from the CMB. Consequently, the

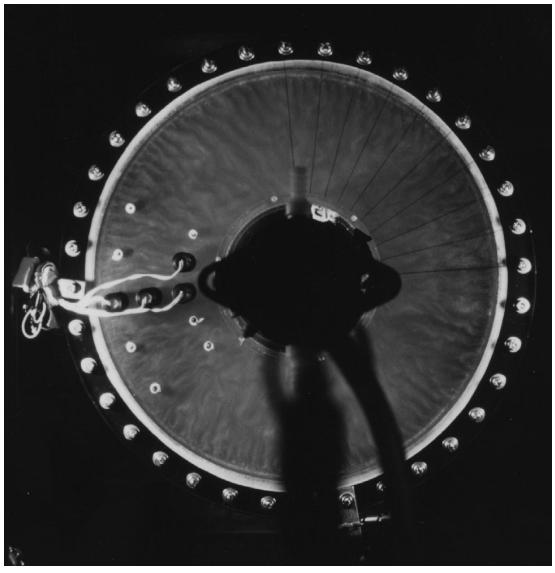

Fig. 6. Turbulent convective pattern visualized by flakes in the dual convection regime at $Ra/Ra_c = 16.6$ ($Ek = 4.7 \times 10^{-6}$).

cells originating from the ICB bifurcate in order to adjust to the larger wave number preferred near the CMB, resulting in turbulence. A similar interpretation has been made by Cordero and Busse (1992) from spectral analysis of temperature fluctuations. Since this style of convection contains two co-existing instabilities with different wave numbers, we call this the *dual convective* regime.

Fig. 7 shows these two instabilities more clearly. Here, the instability from CMB is initiated before the tips of the plumes from the ICB reach the CMB, and before the sphere reaches solid body rotation. This effect is seen only for Ra/Ra_c larger than the penetrative–dual transition, and its final state is identical to that when there is no spin-up effect.

Inspection of the pattern in Fig. 6 shows that in addition to plumes that bifurcate, many of the plumes meander in the radial direction, with about four wavelengths of meander across the shell. Meandering implies that there is a vortex street with alternating cyclonic and anticyclonic vortices along the plume. The plumes originating at the CMB merge as they approach the ICB, and decreases the wave number from 108 near the CMB to about 40 near the ICB. We do not observe a dependence of wave number of the convective cells on Rayleigh number

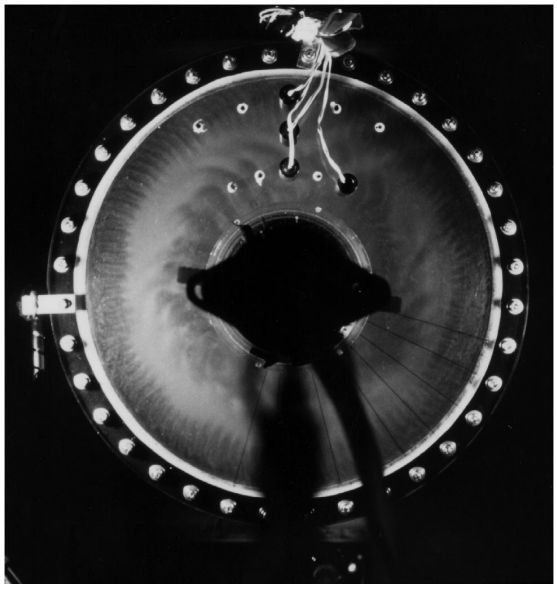

Fig. 7. Dual convection with instabilities formed at opposing boundaries during spin-up at $Ra/Ra_c = 35.9$ ($Ek = 4.7\times10^{-6}$).

over the range of conditions studied. From this behavior, we infer that for a fixed rotation rate, the spherical geometry determines spatial scales of convection in its well-developed state. An interpretative diagram of Fig. 6 is given in Fig. 8.

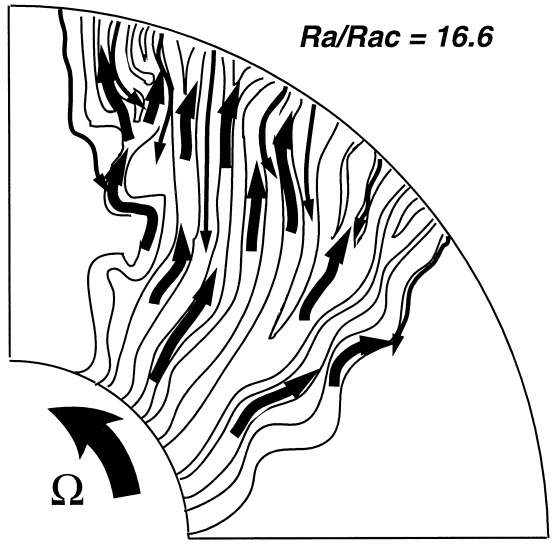

Fig. 8. An interpretive diagram of Fig. 6 showing the fluid motions. The broad (narrow) arrows correspond to cold (warm) plumes emerging from ICB (CMB).

The details of the flow structure is revealed further by using dye tracers. By injecting dye at the CMB, we visualize the individual warm plumes, as seen in Fig. 9. The warm plumes are very thin and are deflected retrograde. These plumes became more vigorous and wider as Rayleigh number is increased. Many of the plumes are seen to extend more than halfway across the shell. Though apparently turbulent in planform, when viewed from oblique angles, these plumes are observed to form two-dimensional dye curtains parallel to the rotational axis, indicating a geostrophic balance. There are, however, some mixing of fluid in and out of the tangential cylinder in this regime, particularly at high Rayleigh number. This was confirmed from observation from oblique angles, and implies that a weak meridional circulation exists.

The zonal flow is similar to that observed in the penetrative convective regime. The region of maximum retrograde flow shifts towards the ICB and its value increases from 5 to 15°/min as Ra/Ra_c increases from 21 to 42. We infer that in the presence of differential rotation, the warm plumes from CMB are more stationary than the cold plumes from ICB.

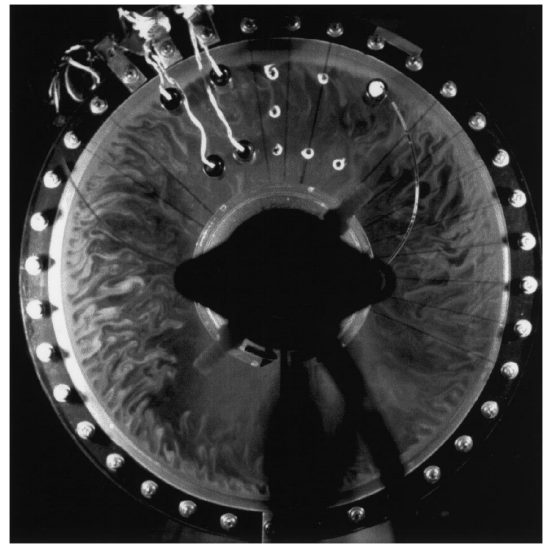

Fig. 9. Dual convection regime visualized by dye at $Ra/Ra_c = 19.3$ ($Ek = 4.7\times10^{-6}$). Dye was released near the CMB, 15 min before this photograph was taken. The dye is denser than the working fluid and spreads along the equatorial CMB, visualizing the fine-scaled warm plume originating from the CMB. The warm plumes have a retrograde tilt, and a wave number of ~ 3 per 10°.

3.2. Thermal structure

3.2.1. Average structure

Fig. 10 compares the measured temperatures for several Rayleigh numbers with conductive profile for the sphere. We can see that in the penetrative convective regime, the measured profile resembles the conductive profile. With increasing Rayleigh number, the interior portion of the shell approaches an isothermal state because of the vigorous convective mixing. The error bars indicate the relative amplitude of temperature fluctuations, which are found to be approximately uniform in magnitude within each of the flow regimes. The uniformity in the amplitude of the temperature fluctuations supports the interpretation that convective structure does not change much with Rayleigh number within a regime. Fig. 10 indicates a general trend towards a larger amplitude fluctuations near the inner core. In relative terms, the magnitude of these fluctuations is proportional to the conductive temperature gradient at the same radius. Accordingly, we infer that differences in the amplitude of the fluctuations reflects radial advection in the background temperature gradient. Comparing records from two probes at the same distance from the axis but at different depths, we find that the amplitude of fluctuations is greater nearer to the equatorial plane, even though the average temperature at each probe is comparable. We interpret this as indicating that convective mixing is most vigorous in the equatorial plane but that the rotation constrains the temperature structure to be nearly cylindrical, especially for high Ra/Ra_c states.

Measurements also show that the temperature at the CMB is lower at 10° latitude than at 50° latitude, by 1–4% of the temperature difference imposed across the hemisphere. There is a slight trend of this

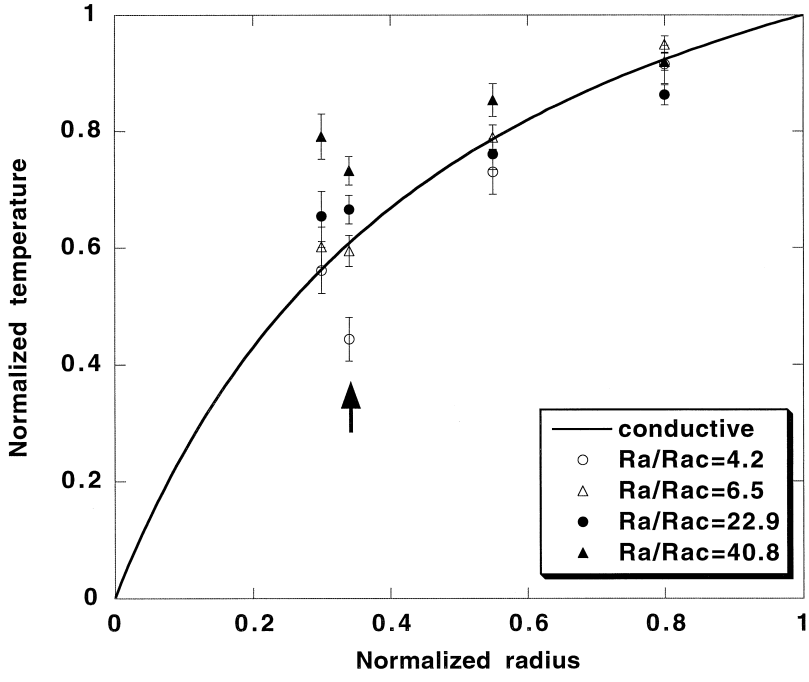

Fig. 10. Radial temperature profile across the shell for several Rayleigh numbers ($Ek = 4.7 \times 10^{-6}$). The temperature and the radius are nondimensionalized by the temperature difference across the shell and the shell thickness. The line indicates the analytical conductive profile. All of the measurements were done at the equatorial plane except the set marked by an arrow, which is at the latitude of 18°, and is at the same distance from the rotation axis as the set closest to the ICB. Open and filled marks represent penetrative and dual convective regimes, respectively. The error bars denote the normalized standard deviation of the fluctuations and are approximately independent of the Rayleigh number. Their values are ~ 4.5, ~ 2.5, ~ 2.8 and $\sim 1.5\%$ with increasing distance from the ICB.

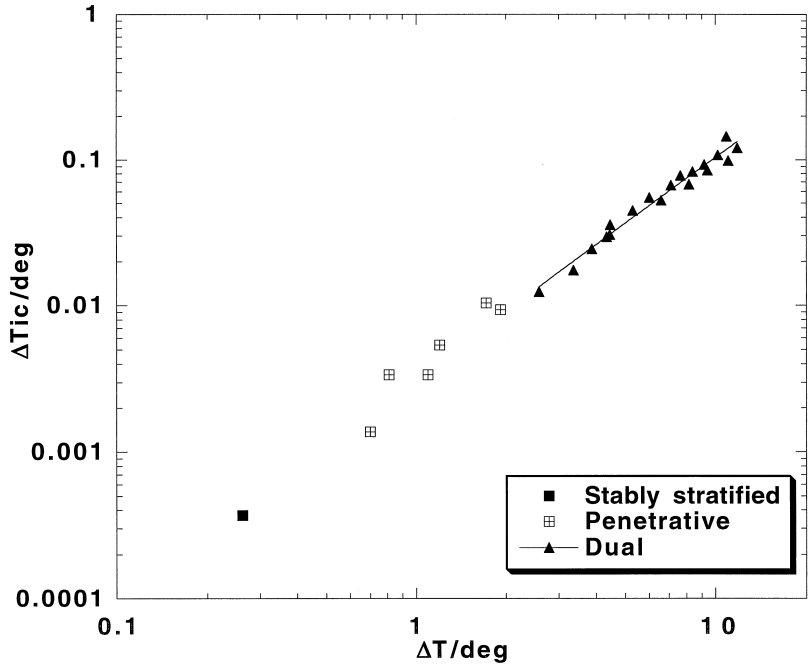

Fig. 11. Heat transfer relations ($Ek = 4.7 \times 10^{-6}$). ΔT: temperature difference between ICB and CMB ($\propto Ra$), ΔT_{ic}: temperature rise of the circulating water in and out of the inner core ($\propto$ total heat flux). The fitted line has a slope of 1.51.

latitude variation to increase with Rayleigh number. These measurements are consistent with the model of cold plumes from the inner core driving the convection, with greatest heat transport near the equatorial plane. This picture is also consistent with a study by Zhang (1992), who showed a two-layered temperature structure and enhanced heat transfer at low latitudes at slightly super-critical Rayleigh number. The preference for this structure at higher Rayleigh numbers has been confirmed by numerical calculations by Glatzmaier and Olson (1993).

A change in heat transfer with increasing Rayleigh number can be inferred from heat flux data in Fig. 11 which shows the relation between the imposed temperature difference ΔT and the temperature increase of the cooling water as it passes through the inner core ΔT_{ic}. Here, the ΔT_{ic} was calculated after correcting for the offset among the two probes in the inner core. The standard deviation of $\Delta T_{ic} \simeq 0.02$°C for all measurements and arises from the temperature fluctuations of the cooling water, and are not shown here. The Rayleigh number dependence of Nusselt number (Nu) can be obtained as follows. Using $\mathrm{Nu} \propto (\Delta T_{ic}/\Delta T)$, $Ra \propto \Delta T$, and fitting the data by $\Delta T_{ic} \propto \Delta T^n$, we get $Nu \propto Ra^{n-1}$. We use the data points in the dual convective regime for fitting, and obtain $Nu \propto Ra^{0.51}$. The magnitude of the total heat flux of the system is $\simeq 16(\Delta T_{ic}/0.1K)$ W, and using this we obtain $Nu = 3.7$ at the penetrative–dual transition ($Ra/Ra_c \simeq 8$) and $Nu = 6.1$ at $Ra/Ra_c = 45$, the maximum Ra in the present experiments. These values indicate that convective heat transfer is important in most of the range covered in the experiment. It is to be remarked that a heat transfer rela-

Fig. 12. Examples of temperature probe time series ($Ek = 4.7 \times 10^{-6}$). (a) Penetrative convection ($Ra/Ra_c = 6.6$) and (b) dual convection ($Ra/Ra_c = 42.2$). The temperature fluctuations are about its mean value, and the measurements of each probe are shifted upwards by (a) 0.25°C and (b) 2°C. The lower three are the measurements in the equatorial plane (from the bottom: inner (0), middle (0), outer (0) of Fig. 1) and the uppermost measurement was made at the same distance from the rotation axis as the lowermost one, but 2.6 cm from the equatorial plane (inner (18) of Fig. 1).

tionship was obtained from numerical calculations at higher Ekman numbers by Tilgner and Busse (1997), who also obtained for $Nu = 1–4$, a larger power-law exponent than the nonrotating convection.

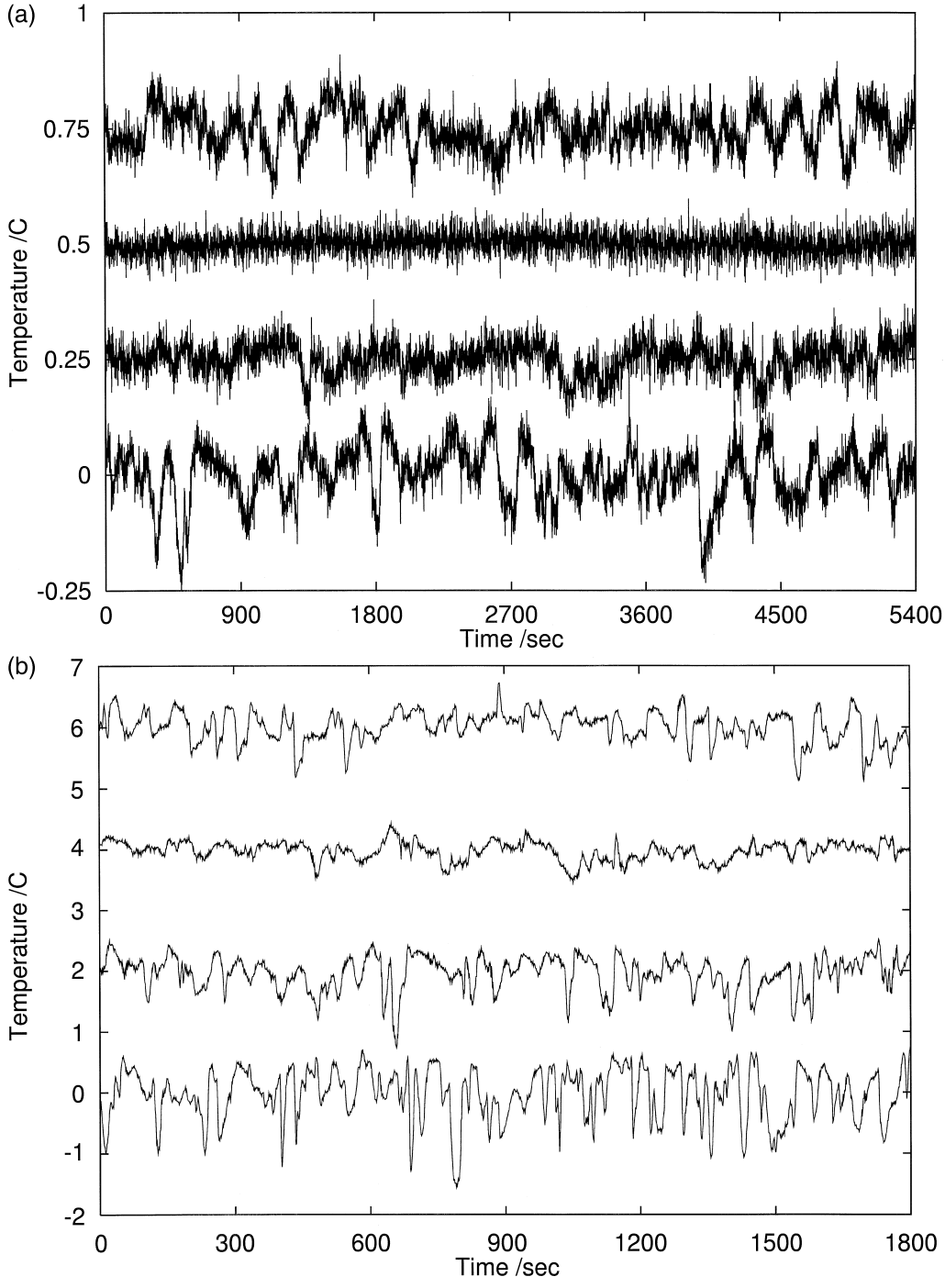

3.2.2. Time-dependent thermal structure

In Fig. 12, we show examples of the records of temperature probe time series around its mean value, at $Ra/Ra_c = 6.6$ in the penetrative regime and at $Ra/Ra_c = 42.2$ in the dual convective regime. Records from four probes placed at different dis-

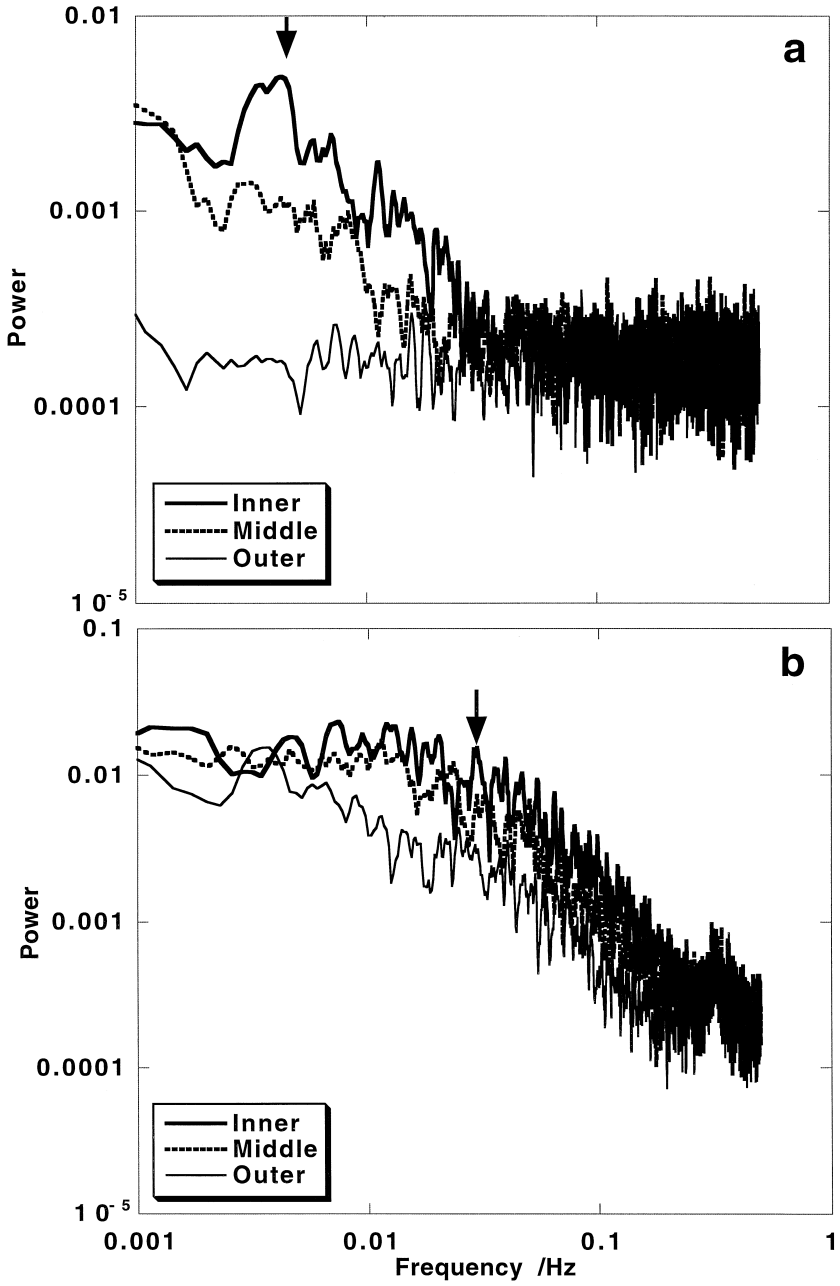

Fig. 13. Temperature power spectra of the records shown in Fig. 12. For location of the probes, see Fig. 1. The data was Hanning filtered and a five-point running average was applied to the spectrum. (a) Penetrative convective ($Ra/Ra_c = 6.6$) and (b) dual convective regimes ($Ra/Ra_c = 42.2$). The peak marked by an arrow corresponds to the retrograde drift of columns.

tances from the ICB and depth from the equatorial plane are shown. The previously discussed trend toward larger amplitude fluctuations near the ICB and near the equatorial plane is evident in this data. At $Ra/Ra_c = 6.6$, for example, Fig. 12 shows irregular fluctuations near the ICB diminishing near the CMB. In the $Ra/Ra_c = 42.2$ case, there are prominent temperature fluctuations throughout the shell. The probe nearest to ICB shows that fluctuations have dominant negative spikes. The typical period of

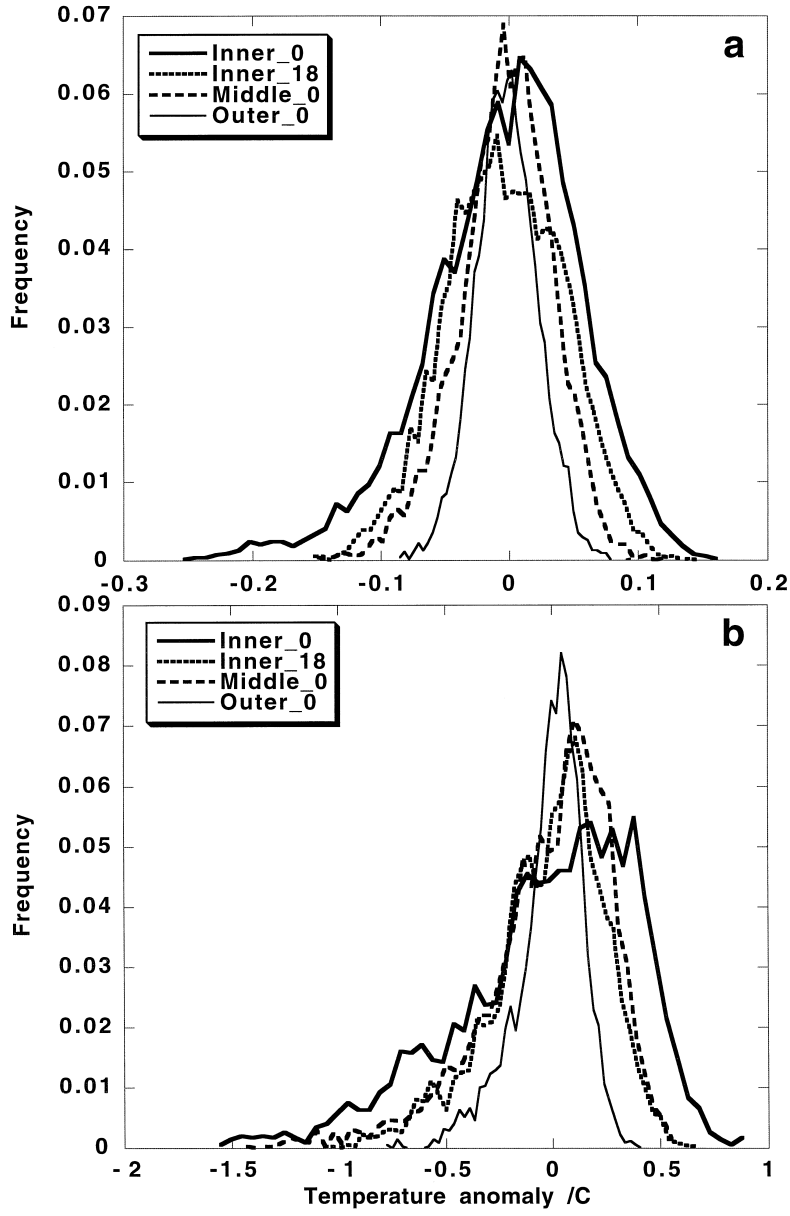

Fig. 14. Histograms of the temperature of the data shown in Fig. 12. For the location of the probes, see Fig. 1. (a) Penetrative convective ($Ra/Ra_c = 6.6$) and (b) dual convective regimes ($Ra/Ra_c = 42.2$). Numbers indicate the latitude of the probe. An asymmetric distribution exists throughout the shell, with large deviation at probes near the ICB and equatorial plane.

the fluctuations clearly decreases with Rayleigh number, from 3–4 min at $Ra/Ra_c = 6.6$ to ~ 40 s at $Ra/Ra_c = 42.2$. We analyze these records in more detail using power spectra and statistical measures.

Fig. 13 shows the Hanning filtered Fourier spectra for each probe at several different Rayleigh numbers. Here, a five-point running average was applied to the spectra. The robust features are as follows. First, the spectrum is white in stably stratified region, for example, the region adjacent to the CMB in the penetrative convection regime. Spectra for the stably stratified regime are similar and are not shown here. Second, the corner frequency at which power starts to decay increases with Rayleigh number. Since the fluctuations are irregular, the spectra often exhibit multiple peaks, some of which seem to be spurious. Therefore, we use corner frequency if there is no well-defined peak. For example, at $Ra/Ra_c \sim 6.6$, a peak exists at ~ 0.0043 Hz near the ICB, which increases to ~ 0.03 Hz at $Ra/Ra_c \sim 44$, as shown by arrows in Fig. 13. It is natural to explain the apparent cyclicity in temperature fluctuations in terms of drifting plumes, which is given by $f \sim 0.0044(V_\phi$ $(^\circ/\mathrm{min})/4)(m/24)$ Hz where V_ϕ is the zonal angular velocity and m is the wave number of the plumes at the radius of interest. The values used here are appropriate for the probe near the ICB at $Ra/Ra_c \sim 6$. Similarly, if we take $V_\phi = 15^\circ/\mathrm{min}$ and $m = 40$ for the case in $Ra/Ra_c \sim 44$, we get $f = 0.028$ Hz. A good agreement we see here supports the interpretation that columns are being advected by zonal flow.

Next, we consider the nonsinusoidal character of the fluctuations. The predominance of negative spikes, which becomes marked as Rayleigh number increases, is a persistent feature, based on the statistical distribution of temperature anomaly around its mean value as shown in Fig. 14. The fluctuations in conductive regions have a Gaussian distribution, whereas in the convective regimes they have an asymmetric distribution, skewed towards the negative values. This asymmetry becomes more pronounced with increasing Rayleigh number. The cold plumes have a larger temperature anomaly than warm plumes because of the nonlinear radial temperature profile.

Another property of the temperature records is that the fluctuations have a saw-tooth pattern with a steep decrease and gradual increase, rather than being sinusoidal. This is not very obvious in the raw records, but is evident in the statistical distribution of the time derivative of the records. The saw-tooth nature of the temperature fluctuations, with rapid decrease followed by a gradual increase, results in more intervals with positive derivative as compared to negative ones, and leads to a distribution with a positive median value. Analyzing the records this way reveals that the median is positive at all probes for both penetrative and dual convective regimes. We interpret this in terms of sampling an array of retrograde drifting cold plumes with enlarged cyclonic circulations. The cyclones tend to become larger than the anticyclones owing to Ekman pumping, and is known from finite amplitude numerical calculations (e.g., Kageyama et al., 1993; Cardin and Olson, 1994; Tilgner and Busse, 1997). In such a case, the temperature minimum would exist at the retrograde side of the symmetrical axis of the cold plumes. A fixed probe sequentially samples temperature in the prograde direction, corresponding to retrograde drift, and this results in a high temperature when sampling across the retrograde side of the cold plume (inward flow) followed by a steep decrease to its minimum and then a gradual increase towards the prograde side the cold plume. If the drift were in the opposite (prograde) direction, or the anticyclones were larger, the behavior would be opposite to what is observed.

4. Discussion

4.1. Flow mechanics

In this section, we offer some explanations for the flow mechanics in the regimes we have identified. We first consider the structure of the radial flow, and then proceed to see how the zonal flow is generated.

In the present experiments, the heat transfer is achieved in terms of radially moving plumes. The heat transfer of these plumes can be evaluated in the following way. From the visual tracking of the dye motions, we estimate a radial velocity $V \sim 1 \times 10^{-3}$ m/s for a warm plume at $Ra/Ra_c = 42$. We can also estimate from the correlation of the pattern of temperature fluctuations among the radially aligned

probes, and obtain $V \sim 2.5 \times 10^{-3}$ m/s for a cold plume at $Ra/Ra_c = 42$. Using this estimate, and taking the length scale as the shell thickness, we find Péclet number $= VL/\kappa \sim 1800$ and Reynolds number $= VL/\upsilon \sim 250$, from which follows the importance of advection over diffusion. Thermal advection supports the large temperature gradients within the fluid, which result in the large amplitudes of the observed temperature fluctuations. The large Péclet number allows for heat transport by fine-scale plumes. For example, the velocity value given above can sustain plume scales of as fine as ~ 2 mm traversing across the shell. In penetrative convection, the convection is driven primarily by prograde tilting cold plumes and the narrow regions of radially inward warm plumes which separates them are return flows. This asymmetric strength of the cold and warm plumes arise from the spherical geometry. The heat flux at ICB and CMB would differ by at least a factor of 3 if we assume an annular heat transfer. Also, assuming an effective gravity $\propto r$, and a temperature distribution $\propto 1/r$, a fluid parcel displaced δr about its position gains a buoyancy $g_{\text{eff}}(\partial T/\partial r)\delta r \propto r(1/r^2) = 1/r$. Combination of these two effects result in the effective buoyancy at ICB to be at least nine times larger than that at CMB, causing the asymmetry we observe.

We now examine the origin of the retrograde zonal flow in the interior. First, we consider the role of angular momentum transfer. There are two ways in which angular momentum transfer is possible (Takehiro and Hayashi, 1995). One is transport towards the equatorial CMB by Reynolds stresses. Prograde flow couples with equatorwards flow and transports positive angular momentum towards the equator. A retrograde flow transports negative angular momentum towards the pole, with the same effect. The prograde spiralling structure as we see in the present experiments will contribute to this further. A second is through the removal of angular momentum from the equatorial CMB by a meridional circulation. In the experiments, there is likely to be a radially outward flow in the equatorial plane. Reynolds stresses spin down the fluid at mid-shell, while the meridional flow mechanisms tend to do the opposite. By inference, Reynolds stresses should overwhelm the meridional flow effects in our experiments. The persistence of a two-dimensional structure also seem to be compatible with weak meridional circulation. It is to be noted, however, that the zonal flow is retrograde for whole region in our experiment, whereas previous theoretical works show prograde flow near the CMB (Busse and Hood, 1982; Zhang, 1992; Cardin and Olson, 1994).

Next, we consider thermal wind, governed by the following relation:

$$2(\Omega \cdot \nabla)\boldsymbol{V} = \alpha \nabla T \times g_{\text{eff}}. \quad (1)$$

Here $\boldsymbol{V}$ is the velocity vector, α is thermal expansivity and g_{eff} is the effective gravity. Assuming a spherically symmetric temperature profile, at mean distance of 0.1 m from axis, the RHS changes its sign at the latitude of 12°, i.e., is negative for latitudes $< 12°$. This implies a relatively retrograde thermal wind with distance from the equatorial plane whose magnitude is, at most, of the order of $\sim 10^{-4}$ $(\Delta T/1\ K)$ m/s, (ΔT: imposed temperature difference across the hemisphere). At the latitude mentioned above, this corresponds to a zonal velocity of $\simeq 3°/\text{min}$. Based on this estimate, it would appear to play a role. However, since the columnar structure of the plumes is always observed, we infer that the contribution from thermal wind with axial shear cannot be very great. Essentially, columnar structure seen in the experiments implies that the Coriolis force predominates over thermal buoyancy, which has already been confirmed by Cardin and Olson (1994). Columnar structure can also be confirmed from temperature measurements. As can be seen from Fig. 12, the typical period of temperature fluctuation of the two thermistor probes situated at the same distance from ICB but at the different distances from the equatorial plane, are similar, which implies that the axial shear of zonal flow must be small in this depth range.

It is of interest to compare the present experimental result with that by Cordero and Busse (1992) who interpreted their fluctuation of temperature signals by superimposition of prograde propagating thermal Rossby wave and retrograde thermal wind. From analyzing in such a way they obtained the prograde propagation rate of thermal Rossby wave equivalent to $\sim 6°/\text{min}$ ($m = 32$, $\Omega = 170$ rpm assumed). In the present experiment, the predicted prograde propagation rate of thermal Rossby wave is ~ 2 or $\sim 5°/\text{min}$, if we apply the linear stability results of

Zhang (1992) and Cardin and Olson (1994), respectively. The inferred thermal wind velocity of Cordero and Busse (1992) and the measured zonal flow rate in our experiments seem to be comparable. In Cordero and Busse's experiments, the relative importance of advection over propagation on drift increases with Rayleigh number. The *retrograde* drift of pattern we observe in the present experiments cannot be explained by *prograde* propagating thermal Rossby waves. We have shown that at $Ra/Ra_c \sim 6$, the velocities of the retrograde drift and of the zonal flow are the same, and that the drift can be explained by advection by zonal flow. This would certainly be so for higher Rayleigh numbers where the zonal flow is faster. We have also shown that this interpretation is compatible with the typical period we observe in the temperature data. It seems that the plume-driven convection as we observe in the experiments is not compatible with the oscillatory particle motion of waves. Furthermore, the very narrow radially inward flow would create a large shear, and would tend to reduce inertia and damp wave motion. The present experiments do not rule out the existence of thermal Rossby waves, but it can be said that advection is the primary cause for drift at most of the parameter range covered here. It is also to be remarked that the thicker shell of the present apparatus, as compared to Cordero and Busse (1992), implies that the effective buoyancy of convection at ICB and CMB is more asymmetrical and that there is a greater tendency for different wave numbers to coexist, which may be responsible for the irregular temperature fluctuations in our experiments.

4.2. Comparison with numerical calculations

Comparison with several numerical studies which deal with a similar system but at a parameter range below the experiments is useful. From calculations at $Ek \sim 10^{-5}$ simulating Jupiter, Zhang and Schubert (1996) found an essentially penetrative style columnar convection. Sun et al. (1993a) report a transition to chaotic convection at $Ra/Ra_c = 5$ and $Ek \sim 10^{-4}$, with high wave number features near the CMB. At lower $Ek \sim 10^{-5}$, they find quasi-layered columnar, highly time-dependent convection with a secondary zonal flow which alternates in direction (Sun et al., 1993b). Tilgner and Busse (1997) from calculations at $Ek \sim 6 \times 10^{-4}$ also show coexistence of different wave numbers and cyclonic enhancement. The general features mentioned above are common to the experimental results shown here. All of the above calculations had a region of prograde zonal flow outside the tangential cylinder. In contrast, a calculation by Glatzmaier and Olson (1993) at $Ek \sim 5 \times 10^{-3}$ produced retrograde flow everywhere, similar to our experiment. Regarding the drift of the pattern, calculations have shown that the drift of the structure becomes highly time-dependent, and that the retrograde drift occurs resulting from zonal flow (e.g., Glatzmaier and Olson, 1993; Kageyama et al., 1993; Sun et al., 1993a,b). This agrees with the experiments in the present paper, where we have shown that the advection by the zonal flow is the main cause for drift in the finite amplitude regimes.

Regarding the resolution of the flow, although calculations contain structures that could be labeled as turbulent, they also tend to produce smoothed flows, because of finite grid size. The use of hyperviscosities in calculations furthers this tendency, as shown by Zhang and Jones (1997). A good test of numerical calculations would be to reproduce large wave number convection such as shown in Fig. 9.

4.3. Geophysical implications

From the experimental results shown here, several new regimes of convection in the Earth's core seem possible. The key assumption is that the force balance in the core is primarily geostrophic. We have found three different styles of flow, depending on Ra/Ra_c. Since little is known about the actual Ra/Ra_c in the Earth's core, both globally and locally, each of these styles is possible. The stably stratified regime is relevant to regions in the Earth's core where the temperature gradient is sub-adiabatic or the fluid is compositionally stratified. The experiments show that within such region, the flow is not completely static, instead zonal flows in the form of interleaving lenses exist. The penetrative convective regime corresponds to the case when the convection beneath the CMB is suppressed by stable stratification. Stable stratification can exist near the CMB for thermal (Gubbins et al., 1982) or compositional (Fearn and Loper, 1981) reasons, and has been inferred seismologically (Lay and Young, 1990). Our

experiments show that, in this case, an array of spiralling columnar plumes from the ICB is the primary style of convection. The dual convective regime occurs when the buoyancy is so large that vigorous convection occurs throughout the core, driven by both plumes rising from ICB and descending from CMB. In both convective regimes seen in our experiments, the flow is plume-driven. An essentially two-dimensional columnar structure is always observed, even for high Ra/Ra_c, and the magnitude of the poloidal flow always exceeded the toroidal flow in the region outside the inner core tangent cylinder. These features are also likely to be common in the Earth's core as well. Turbulence is produced by interaction of plumes from the opposing boundaries, and can become one of the reasons for the turbulence in the Earth's core.

The experiments also show new ways of interpreting the geomagnetic data. If bifurcation of the columnar plumes, as seen in Fig. 4, occurs in the Earth's core, this may be apparent in the form of short wave length flux patches becoming prominent at low latitudes. We have shown that nonsinusoidal features of temperature fluctuations measured by a single probe, reflect nonlinear temperature profile and asymmetricity in the size of cyclonic and anticyclonic vortices. Perhaps, the secular variation of the geomagnetic field could be analyzed in a similar way for interpreting convection in the core. Regarding the retrograde drift of pattern, experimental results show that this is primarily due to the zonal flow rather than wave motions in the fluid, which are inhibited when the flow is dominated by plumes.

5. Conclusions

Three distinct flow regimes are found at $Ek = 4.7 \times 10^{-6}$ and for Ra/Ra_c up to 45.

- $Ra/Ra_c < 1$, *Stably stratified*: a slow zonal flow in the shell interior exists, consisting of interleaved lenses of retrograde and prograde motion.
- $1 < Ra/Ra_c < 8$, *Penetrative convection*: the convection consists of closely spaced prograde spiralling cold plumes which originate at the ICB and penetrate to the outer portion of the shell. When fully developed, the plumes extend to the CMB. They have an azimuthal wave number of $m = 24$ near ICB, and bifurcate in radius so that $m = 70$ near the CMB. The radial flow exceeds the zonal flow. The mean zonal flow is retrograde at $\sim 4^\circ$/min, and the plumes slowly drift retrograde at the same rate, due to the advection by mean zonal flow, rather than from wave motion. Temperature fluctuations with dominant negative spikes are observed, reflecting pronounced radially outward heat transfer in the equatorial plane, and irregular drift. The columnar structure of the convection is persistent. The thermal structure is similar to conductive profile in this regime.
- $Ra/Ra_c > 8$, *Dual convection*: the convection remains essentially two-dimensional and consists of two parts — (i) the cold plumes from the ICB, and (ii) fine-scale warm plumes from the CMB. The plumes at CMB are triggered by arrival of the cold plumes originating at the ICB and have azimuthal wave number $m = 108$. Discrepancy between the wave numbers of these plumes results in turbulence, in the form of bifurcation and meandering of plumes. A mean retrograde flow also occurs in this regime. The temperature field approaches isothermal in the interior region of the shell due to mixing, and the convection dominates the heat transfer. Time scale of temperature fluctuations becomes shorter, indicating faster advection of small-scale columnar structures by the azimuthal flow.

Acknowledgements

We thank P. Cardin for discussions, K. Zhang and two anonymous referees for helpful comments on the manuscript. I.S. is supported by JSPS Research Fellowships for Young Scientists. The experiments were supported through the Geophysics Program of NSF.

References

Busse, F.H., 1970. Thermal instabilities in rapidly rotating systems. J. Fluid Mech. 44, 441–460.

Busse, F.H., Hood, L.K., 1982. Differential rotation driven by a convection in a rapidly rotating annulus. Geophys. Astrophys. Fluid Dyn. 21, 59–74.

Busse, F.H., Hartung, G., Jaletzky, M., Sommerman, G., 1997. Experiments on thermal convection in rotating systems moti-

vated by planetary problems. Dynamics of Atmospheres and Oceans 27, 161–174.

Cardin, P., Olson, P., 1992. An experimental approach to thermochemical convection in the Earth's core. Geophys. Res. Lett. 19, 1995–1998.

Cardin, P., Olson, P., 1994. Chaotic thermal convection in a rapidly rotating spherical shell: consequences for flow in the outer core. Phys. Earth Planet. Inter. 82, 235–259.

Cordero, S., 1993. Experiments on convection in a rotating hemispherical shell: transition to chaos. Geophys. Res. Lett. 20, 2587–2590.

Cordero, S., Busse, F.H., 1992. Experiments on convection in rotating hemispherical shells: transition to a quasi-periodic state. Geophys. Res. Lett. 19, 733–736.

Fearn, D.R., Loper, D.E., 1981. Compositional convection and stratification of Earth's core. Nature 289, 393–394.

Glatzmaier, G.A., Olson, P., 1993. Highly supercritical thermal convection in a rotating spherical shell: centrifugal vs. radial gravity. Geophys. Astrophys. Fluid Dyn. 70, 113–136.

Gubbins, D., Thomson, C.J., Whaler, K.A., 1982. Stable regions in the Earth's liquid core. Geophys. J. R. Astron. Soc. 68, 241–251.

Kageyama, A., Watanabe, K., Sato, T., 1993. Simulation study of a magnetohydrodynamic dynamo: convection in a rotating spherical shell. Phys. Fluids B 5, 2793–2805.

Lay, T., Young, C.J., 1990. The stably-stratified outermost core revisited. Geophys. Res. Lett. 17, 2001–2004.

Manneville, J.-B., Olson, P., 1996. Banded convection in rotating fluid spheres and the circulation of the Jovian atmosphere. Icarus 122, 242–250.

Sun, Z.-P., Schubert, G., Glatzmaier, G.A., 1993a. Transitions to chaotic thermal convection in a rapidly rotating spherical fluid shell. Geophys. Astrophys. Fluid Dyn. 69, 95–131.

Sun, Z.-P., Schubert, G., Glatzmaier, G.A., 1993b. Banded surface flow maintained by convection in a model of the rapidly rotating giant planets. Science 260, 661–664.

Takehiro, S., Hayashi, Y.-Y., 1995. Boussinesq convection in rotating spherical shells — a study on the equatorial superrotation. In: Yukutake, T. (Ed.), The Earth's Central Part: Its Structure and Dynamics. Terra Scientific Publishing, Tokyo, pp. 123–156.

Tilgner, A., Busse, F.H., 1997. Finite-amplitude convection in rotating spherical fluid shells. J. Fluid Mech. 332, 359–376.

Zhang, K., 1992. Spiralling columnar convection in rapidly rotating spherical fluid shells. J. Fluid Mech. 236, 535–556.

Zhang, K., Schubert, G., 1996. Penetrative convection and zonal flow on Jupiter. Science 273, 941–943.

Zhang, K., Jones, C.A., 1997. The effect of hyperviscosity on geodynamo models. Geophys. Res. Lett. 24, 2869–2872.